JOURNAL OF GUIDANCE, CONTROL, AND DYNAMICS
Vol. 30, No. 5, September–October 2007

Long-Term Attitude Drift of Spinning Spacecraft Under Solar Radiation Torques

Jozef C. van der Ha*
Kyushu University, Fukuoka 817-0395, Japan
and
Vaios J. Lappas†
Surrey Space Centre, Guildford, GU2 7XH England, United Kingdom

DOI: 10.2514/1.28506

Solar radiation pressure effects have been exploited by satellites for about four decades. Concepts have been developed for using solar radiation forces and torques in practical applications, for instance, for orbit stationkeeping and attitude stabilization of geostationary communications satellites. The forces and torques induced by solar radiation pressure can substantially alter the orbital and attitude behavior of spacecraft, especially in long-duration missions. The present work analyzes the long-term effect of the solar radiation torques on the evolution of the spin-axis attitude pointing of any type of spacecraft (e.g., Earth-orbiting spacecraft, deep space probes, and solar sails). Analytic models are presented that can be applied to a spacecraft of an arbitrary geometrical shape. Compact results are established that predict the annual drift of the spacecraft spin axis under solar radiation torques. The models presented will be useful for the design of spacecraft attitude control systems as well as for space mission planning, including hibernation concepts.

Nomenclature

A	=	area of spacecraft surface element under consideration, m^2
C	=	constant
c_m, c_p	=	center of mass, center of pressure
c_{ak}^m, s_{ak}^m	=	Fourier coefficients
c_0	=	cosine of $\lambda_\odot(d_0)$
d	=	time, days
d_γ	=	epoch of the vernal equinox
$\mathbf{F}$	=	solar radiation force
$\mathbf{f}_a$, $\mathbf{f}_d$, $\mathbf{f}_s$	=	absorptive, diffuse, and specular parts of the solar radiation force
f_{ak}, f_{dk}, f_{sk}	=	functions
f_1, f_2	=	force terms
g	=	threshold
g_1, g_2	=	torque terms
h	=	height of the spacecraft, m
I_z	=	moment of inertia about the spin axis, kg m^2
$\mathbf{n}$	=	unit-vector normal to the surface element
n_x, n_y, n_z	=	components of $\mathbf{n}$ along the spacecraft axes
P	=	solar radiation force parameter, pA/R^2, N
p	=	solar radiation pressure, $p \approx 4.56 \times 10^{-6}$, N/m^2
Q	=	angular rate
R	=	distance from the spacecraft to the sun, AU
r	=	length of the lever arm of the solar radiation pressure torque
$\mathbf{r}$	=	lever-arm vector of the solar radiation pressure torque
r_{cyl}	=	radius of the cylindrical spacecraft
r_x, r_y, r_z	=	components of $\mathbf{r}$ along the spacecraft axes
$\mathbf{s}$	=	sun unit vector (from the spacecraft to the sun)
s_0	=	sine of $\lambda_\odot(d_0)$
s_1, s_2, s_3	=	components of $\mathbf{s}$ along the inertial X, Y, and Z axes
T	=	solar radiation torque magnitude
$\mathbf{T}$	=	solar radiation torque vector
t	=	time, s
$\mathbf{t}_a$, $\mathbf{t}_d$, $\mathbf{t}_s$	=	absorptive, diffuse, and specular parts of solar radiation torque
W	=	modified angular rate, $W = Q \sin\gamma_{\text{ave}}/\omega_\odot$
w	=	precession rate, rad/s
$\mathbf{w}$	=	precession vector
X, Y, Z	=	Earth-centered inertial reference frame
$\mathbf{x}$, $\mathbf{y}$, $\mathbf{z}$	=	unit vectors along the x, y, and z axes
x, y, z	=	spacecraft body reference frame with z as the spin axis
x_s, y_s, z_s	=	sun-spin-axis reference frame
$\mathbf{x}_s$, $\mathbf{y}_s$, $\mathbf{z}_s$	=	unit vectors along the x_s, y_s, and z_s axes
$\mathbf{z}$	=	unit vector along the spin axis
$\mathbf{z}_0$	=	initial value of the spin-axis direction
z_1, z_2, z_3	=	inertial components of spin-axis direction $\mathbf{z}$
z_{10}, z_{20}, z_{30}	=	inertial components of the initial spin-axis direction
α, δ	=	right ascension and declination of the spin axis in the inertial frame
γ	=	solar aspect angle
γ_{ave}	=	averaged solar aspect angle over a year
Δ	=	infinitesimal change
Δt	=	spin period (considered infinitesimal)
ε	=	misalignment angle
$\varepsilon_\odot$	=	ecliptic obliquity
ϑ	=	precession angle
$\lambda_\odot$	=	sun's ecliptic longitude
μ, ν	=	right ascension and declination of normal $\mathbf{n}$ in the spacecraft frame
ξ, η, ζ	=	components of the spin axis along the ecliptic frame
ρ	=	specular reflectivity coefficient
σ	=	diffuse reflectivity coefficient
φ	=	constant
χ, τ	=	right ascension and declination of the lever arm in the spacecraft frame

Presented as Paper 415 at the AAS/AIAA Astrodynamics Conference, Lake Tahoe, CA, 7–11 August 2005; received 23 October 2006; revision received 27 March 2007; accepted for publication 27 March 2007.

*Professor, Department of Aeronautics and Astronautics; jvdha@aol.com. Senior Member AIAA.

†Lecturer, Attitude/Orbit Control Systems; V.Lappas@surrey.ac.uk.

ψ	=	spin-phase angle
$\bar{\psi}$, $\hat{\psi}$	=	modified spin-phase angles, $\psi + \nu$ and $\psi + \tau$, respectively
ω	=	spacecraft spin rate, rad/s
$\omega_\odot$	=	sun's mean angular rate, deg /day

Subscripts

a	=	absorptive component
ave	=	averaged value over a year
d	=	diffuse component
i	=	index of the surface element
max	=	maximum value over a year
s	=	specular component
x, y, z	=	components along the spacecraft axes
0	=	initial condition
1, 2	=	start and end of the averaging interval

Superscripts

$\cdot$	=	differentiation with respect to time, s
$'$	=	differentiation with respect to time, days

I. Introduction

SOLAR radiation pressure (SRP) effects on satellites have been studied extensively during the last 45 years [1–5]. Spacecraft attitude and orbit control systems must compensate for the SRP disturbances throughout the mission lifetime. On the other hand, SRP effects can also be exploited for specific attitude and orbit control objectives. In any case, a good understanding and accurate prediction of the SRP effects is important during the mission design and can lead to reductions in the required onboard propellant.

The concept of using SRP torques for attitude stabilization was first raised in 1959 by Sohn [1]. The technique has successfully been implemented in a variety of space missions, but especially in geostationary communications satellites. For instance, OTS, INSAT, TELECOM 1, and INMARSAT 2 make use of the windmill torques induced by SRP to perform roll/yaw attitude stabilization [2–4]. The orientation of the north and south solar arrays can be rotated differentially (about the pitch axis) with respect to the nominal sun-pointing orientation. In this manner, disturbance torques about the roll and yaw axes can be countered without expenditure of onboard propellant. Wie [3,4] presented the dynamics and control of solar sails under SRP effects, showing that the offset between the center of mass and center of pressure can cause attitude control and stability problems. With regard to orbital effects caused by SRP, van der Ha and Modi [5] provided a model for predicting the effects on space structures of arbitrary geometrical shape.

Patterson and Kissel [6] examined the effects of SRP on the PAGEOS balloon spacecraft and observed a highly variable rotation rate and a precession of its spin axis. They used an ellipsoidal model to explain these variations. Pande [7] considered the possibility of using SRP to develop a controller to rotate the spin axis of a spacecraft using two solar panels along its spin axis. The controller was shown to be able to rotate the spin axis of a medium-sized spacecraft from the orbit normal attitude to the in-orbit plane orientation (i.e., a 90-deg rotation angle) in about four days. Parvez [8] examined the SRP disturbance on the GSTAR and SPACENET spacecraft and estimated the SRP torque at different times of the year using the in-orbit performance of the momentum wheels and the duty cycle of the magnetic torquers. Their results have been used in preparing stationkeeping maneuvers and also in the validation of SRP models used in the design of the attitude control system. Ziebart [9] provided a detailed analytic formulation for SRP modeling of spacecraft with complex shapes. Rios-Reyes and Scheeres [10] presented a generalized methodology for the analytic description of the forces and moments generated by a solar sail of arbitrary shape and optical properties.

The model presented in this paper offers predictions of the long-term drift of the spin axis of a spin-stabilized spacecraft under the influence of SRP torques. Analytic expressions for the SRP force and torque effects are found by summing the various spacecraft surface areas, each with its own reflective properties and its position and orientation relative to the spin axis. The long-term evolution of the spin-axis-pointing direction is established by means of an averaging operation over the spin revolution. This leads to practical compact models that can predict the evolution of the attitude drift of an arbitrary spacecraft configuration under SRP torques. A few practical applications with primary relevance for the attitude pointing of deep space probes during their hibernation periods are presented for illustration.

II. Spacecraft and Sun Geometry

Figure 1 shows the orientation of the instantaneous spacecraft reference frame (x, y, z) within the Earth-centered inertial reference frame (X, Y, Z). The spacecraft x and y axes rotate rapidly about the z axis under the spacecraft spin rate, which is typically within the range from a few rpm up to perhaps 120 rpm. The spacecraft spin axis (i.e., the z axis), on the other hand, moves very slowly in inertial space under the action of external torques.

The instantaneous orientation of the spacecraft spin axis in the inertial geocentric reference frame (X, Y, Z) is described by the unit vector $\mathbf{z} = (z_1, z_2, z_3)^T$ with

$$z_1 = \cos\alpha\cos\delta; \qquad z_2 = \sin\alpha\cos\delta; \qquad z_3 = \sin\delta \tag{1}$$

The instantaneous sun position within the inertial frame (Fig. 1) is defined by the unit vector $\mathbf{s}$ with components $\mathbf{s} = (s_1, s_2, s_3)^T$. The evolution of the sun unit vector in the geocentric equatorial frame can be described by the analytical model presented by Vallado [11]:

$$s_1 = \cos\lambda_\odot; \qquad s_2 = \sin\lambda_\odot\cos\varepsilon_\odot; \qquad s_3 = \sin\lambda_\odot\sin\varepsilon_\odot \tag{2}$$

The sun's ecliptic longitude $\lambda_\odot$ and the ecliptic obliquity $\varepsilon_\odot$ are given by the approximate expressions (with acceptable accuracy for the long-term applications to be considered here):

$$\lambda_\odot \approx \omega_\odot(d - d_\gamma); \qquad \varepsilon_\odot \approx 23.439 \text{ deg} \tag{3}$$

Time is expressed in terms of days relative to the epoch of the vernal equinox. The sun's mean angular rate of $\omega_\odot \approx 0.9856$ deg /day in the inertial geocentric frame is extremely small compared with the spin rate ω.

Figure 2 shows the geometry of the sun vector relative to the spacecraft spin axis, which is characterized by the instantaneous solar aspect angle γ. The instantaneous sun-spin-axis plane is defined by the unit vectors $\mathbf{s}$ and $\mathbf{z}$ toward the sun and along the spin axis, respectively. This plane contains the x_s and z_s coordinate axes, and the latter axis is pointing along the spin axis (Fig. 2). The unit vectors $\mathbf{x}_s$ and $\mathbf{y}_s$ follow from the geometry in Fig. 2 and can be expressed in the known unit vectors $\mathbf{s}$ and $\mathbf{z}$:

$$\mathbf{x}_s = (\mathbf{s} - \cos\gamma\,\mathbf{z})/\sin\gamma; \qquad \mathbf{y}_s = \mathbf{z} \times \mathbf{x}_s \tag{4}$$

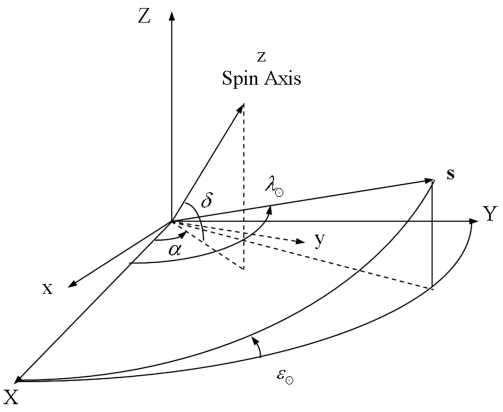

Fig. 1 Geometry of the spacecraft frame and sun motion in inertial space.

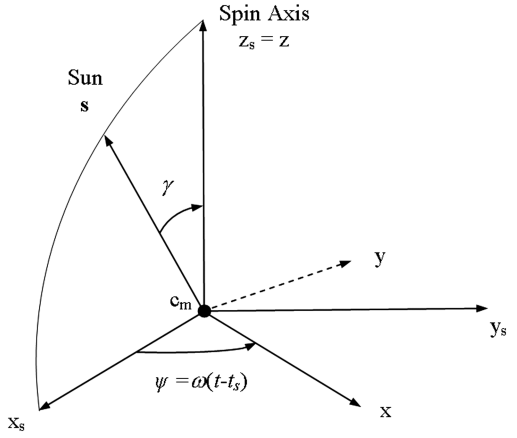

Fig. 2 Geometry of the sun-spin-axis plane x_s–z_s.

Thus, the y_s axis points normal to the instantaneous sun-spin-axis plane.

It should be noted that the (x_s, y_s, z_s) sun-spin-axis frame is not strictly inertial, because it is defined by the sun vector and the spin axis, both of which are slowly varying in time. Nevertheless, during the relatively short duration of one spacecraft revolution, we may consider this frame to be *quasi inertial* or *frozen*. For illustration, typical spin rates of operational satellites are in the range from 5 to 120 rpm, and so one revolution would take between 0.5 and 12 s. This is very fast compared with the slow changes in the spacecraft attitude orientation and in the sun vector's inertial position. The slow variation of the sun-spin-axis plane provides the justification for eliminating the fast spin motion from the long-term effects by means of spin-averaging of the solar radiation forces and torques.

When using the definitions in Eqs. (1) and (2), we can write the solar aspect angle as

$$\gamma = \arccos(\mathbf{z}\cdot\mathbf{s}) = \arccos\{C\cos(\lambda_\odot - \varphi)\} \tag{5}$$

with

$$\begin{aligned} C &= \left\{z_1^2 + [z_2\cos\varepsilon_\odot + z_3\sin\varepsilon_\odot]^2\right\}^{1/2} \\ \varphi &= \tan^{-1}\{[z_2\cos\varepsilon_\odot + z_3\sin\varepsilon_\odot]/z_1\} \end{aligned} \tag{6}$$

Two specific attitude orientations are of particular interest: namely, those defined by the vectors $\mathbf{z}^+$ and $\mathbf{z}^-$:

$$\mathbf{z}^+ = (0, -\sin\varepsilon_\odot, \cos\varepsilon_\odot)^T; \qquad \mathbf{z}^- = -\mathbf{z}^+ \tag{7}$$

Equation (6) shows that the amplitude C vanishes and the angle φ is ill-defined for both of these vectors. From Eq. (5), we find that the solar aspect angle is $\gamma^{+/-} = 90$ deg while these vectors are pointing north and south to the ecliptic plane. These specific attitude orientations are of considerable practical interest for hibernating deep space probes during their long cruise phases in a near-ecliptic trajectory. They offer favorable operational conditions, because the solar aspect angle may be maintained close to 90 deg throughout the hibernation phase without any active control [12].

For the spinning satellite applications considered here, the spacecraft frame (x, y, z) rotates about the $z = z_s$ axis, which is assumed to remain fixed during one spin period. The transformation between the spacecraft (x, y) axes and the quasi-inertial (x_s, z_s) axes (Fig. 2) can be expressed in terms of the spin-phase angle $\psi(t) = \omega(t - t_s)$, with ω denoting the spin rate and t_s denoting the instant at which the spacecraft x axis crosses the sun-spin-axis plane:

$$\begin{pmatrix} x \\ y \end{pmatrix} = \begin{bmatrix} \cos\psi(t) & \sin\psi(t) \\ -\sin\psi(t) & \cos\psi(t) \end{bmatrix} \begin{pmatrix} x_s \\ y_s \end{pmatrix} \tag{8}$$

III. Solar Radiation Force Model

A. General Force Model

For many space missions, the solar radiation effect represents the dominant environmental force. The solar radiation pressure acting on a flat-surface area A induces a force $\mathbf{F}$ that can be written [3–5,13] in components along the unit vectors $\mathbf{s}$ and $\mathbf{n}$:

$$\mathbf{F} = -P(\mathbf{n}\cdot\mathbf{s})\{(1-\rho)\mathbf{s} + [\sigma + 2\rho(\mathbf{n}\cdot\mathbf{s})]\mathbf{n}\} \quad \text{if } (\mathbf{n}\cdot\mathbf{s}) > 0 \tag{9a}$$

$$\mathbf{F} = \mathbf{0} \quad \text{if } (\mathbf{n}\cdot\mathbf{s}) \le 0 \tag{9b}$$

When studying the effects of solar radiation pressure, we may replace an arbitrary satellite body by a number of flat-surface elements A_i $(i = 1, 2, \ldots,)$, each with its own normal $\mathbf{n}_i$, its own (homogeneous) material properties ρ_i and σ_i, and its resulting solar radiation force $\mathbf{F}_i$. The total solar radiation force on the satellite equals the sum of the individual forces $\mathbf{F} = \Sigma_i\,(\mathbf{F}_i)$, where each of the $\mathbf{F}_i$ is given by the force expression of Eq. (9a) with the specific parameters for the surface A_i.

B. Force in the Sun-Spin-Axis Frame

The force expression in Eq. (9a) can be reformulated in a more opportune form:

$$\mathbf{F} = -P\{(1-\rho)\mathbf{f}_a + \sigma\mathbf{f}_d + 2\rho\mathbf{f}_s\} \quad \text{if } (\mathbf{n}\cdot\mathbf{s}) > 0 \tag{10}$$

The vectors $\mathbf{f}_a$, $\mathbf{f}_d$, and $\mathbf{f}_s$ refer to the absorptive, diffuse, and specular contributions to the solar radiation force:

$$\mathbf{f}_a = (\mathbf{n}\cdot\mathbf{s})\mathbf{s}; \qquad \mathbf{f}_d = (\mathbf{n}\cdot\mathbf{s})\mathbf{n}; \qquad \mathbf{f}_s = (\mathbf{n}\cdot\mathbf{s})^2\mathbf{n} \tag{11}$$

In the present model, the solar radiation force will be formulated in components along the quasi-inertial sun-spin-axis reference frame. Therefore, the normal $\mathbf{n}$ to the surface element A must be transformed to this frame. First, the components of $\mathbf{n}$ are expressed in its declination $\mu = \arcsin(n_z)$ and right ascension $\nu = \arctan(n_y/n_x)$ relative to the x, y, and z spacecraft axes (Fig. 3):

$$\mathbf{n} = \cos\mu\cos\nu\,\mathbf{x} + \cos\mu\sin\nu\,\mathbf{y} + \sin\mu\,\mathbf{z} \tag{12}$$

The rotation of the spacecraft frame within the sun-spin-axis frame (Fig. 2) is described by the spin-phase angle ψ based on the transformation between the two frames in Eq. (8), and the transformed normal vector becomes

$$\mathbf{n}(\tilde{\psi}) = \cos\mu\cos\tilde{\psi}\,\mathbf{x}_s + \cos\mu\sin\tilde{\psi}\,\mathbf{y}_s + \sin\mu\,\mathbf{z}_s \tag{13}$$

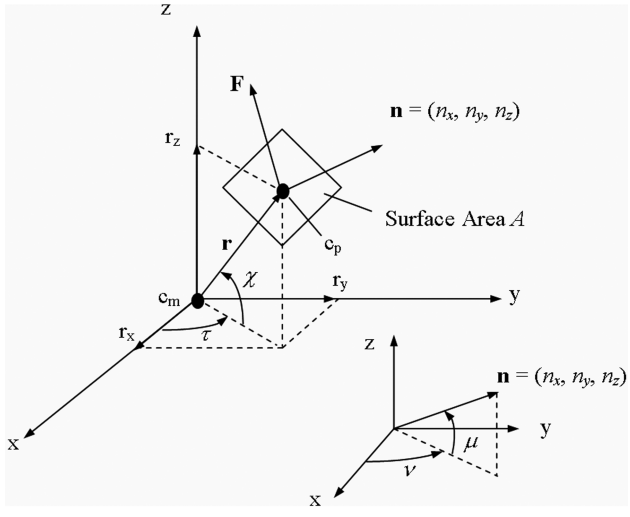

Fig. 3 Solar radiation pressure force on a surface element.

The components of the sun vector in the sun-spin-axis frame can be found from Fig. 2:

$$\mathbf{s} = \sin\gamma\,\mathbf{x}_s + \cos\gamma\,\mathbf{z}_s \tag{14}$$

The instantaneous inner product of $\mathbf{n}$ and $\mathbf{s}$ follows as

$$(\mathbf{n}\cdot\mathbf{s}) = \sin\gamma\cos\mu\cos\tilde{\psi} + \cos\gamma\sin\mu \tag{15}$$

To evaluate the vectors $\mathbf{f}_a$, $\mathbf{f}_d$, and $\mathbf{f}_s$ in Eq. (11), we use the results from Eqs. (13–15):

$$\mathbf{f}_a = (\mathbf{n}\cdot\mathbf{s})\mathbf{s} = f_{ax}(\tilde{\psi})\mathbf{x}_s + f_{az}(\tilde{\psi})\mathbf{z}_s = (\cos\gamma\sin\mu + \sin\gamma\cos\mu\cos\tilde{\psi})\{\sin\gamma\,\mathbf{x}_s + \cos\gamma\,\mathbf{z}_s\} \tag{16a}$$

$$\begin{aligned}\mathbf{f}_d &= (\mathbf{n}\cdot\mathbf{s})\mathbf{n} = f_{dx}(\tilde{\psi})\mathbf{x}_s + f_{dy}(\tilde{\psi})\mathbf{y}_s + f_{dz}(\tilde{\psi})\mathbf{z}_s \\ &= \cos\mu\{\cos\gamma\sin\mu\cos\tilde{\psi} + \sin\gamma\cos\mu\cos^2\tilde{\psi}\}\mathbf{x}_s \\ &\quad + \cos\mu\{\cos\gamma\sin\mu\sin\tilde{\psi} + \tfrac{1}{2}\sin\gamma\cos\mu\sin(2\tilde{\psi})\}\mathbf{y}_s \\ &\quad + \sin\mu\{\cos\gamma\sin\mu + \sin\gamma\cos\mu\cos\tilde{\psi}\}\mathbf{z}_s\end{aligned} \tag{16b}$$

$$\begin{aligned}\mathbf{f}_s &= (\mathbf{n}\cdot\mathbf{s})^2\mathbf{n} = f_{sx}(\tilde{\psi})\mathbf{x}_s + f_{sy}(\tilde{\psi})\mathbf{y}_s + f_{sz}(\tilde{\psi})\mathbf{z}_s \\ &= \cos\mu\{\cos^2\gamma\sin^2\mu\cos\tilde{\psi} + \tfrac{1}{2}\sin(2\gamma)\sin(2\mu)\cos^2\tilde{\psi} \\ &\quad + \sin^2\gamma\cos^2\mu\cos^3\tilde{\psi}\}\mathbf{x}_s + \cos\mu\{\cos^2\gamma\sin^2\mu\sin\tilde{\psi} \\ &\quad + \tfrac{1}{4}\sin(2\gamma)\sin(2\mu)\sin(2\tilde{\psi}) + \sin^2\gamma\cos^2\mu\sin\tilde{\psi}\cos^2\tilde{\psi}\}\mathbf{y}_s \\ &\quad + \sin\mu\{\cos^2\gamma\sin^2\mu + \tfrac{1}{2}\sin(2\gamma)\sin(2\mu)\cos\tilde{\psi} \\ &\quad + \sin^2\gamma\cos^2\mu\cos^2\tilde{\psi}\}\mathbf{z}_s\end{aligned} \tag{16c}$$

The functions $f_{ak}(\tilde{\psi})$, $f_{dk}(\tilde{\psi})$, and $f_{sk}(\tilde{\psi})$, with $k = x, y, z$, are defined by the detailed expressions on the right-hand sides of Eq. (16). They are periodic functions of $\tilde{\psi}$ and can be expressed in the form of a Poisson series:

$$f_{ak}(\tilde{\psi}) = c^0_{ak} + c^1_{ak}\cos(\tilde{\psi}) \qquad (k = x, z) \tag{17a}$$

$$f_{dk}(\tilde{\psi}) = c^0_{dk} + \sum_{m=1}^{2}\left\{c^m_{dk}\cos(m\tilde{\psi}) + s^m_{dk}\sin(m\tilde{\psi})\right\} \qquad (k = x, y, z) \tag{17b}$$

$$f_{sk}(\tilde{\psi}) = c^0_{sk} + \sum_{m=1}^{3}\left\{c^m_{sk}\cos(m\tilde{\psi}) + s^m_{sk}\sin(m\tilde{\psi})\right\} \qquad (k = x, y, z) \tag{17c}$$

It follows that the average value of $f_{ak}(\tilde{\psi})$ over the full spin period equals c^0_{ak}, and similar results hold for the other functions. In general, however, the solar radiation force acts only over a part of the spin revolution: namely, when $(\mathbf{n}\cdot\mathbf{s}) > 0$ [Eqs. (9) and (10)]. Therefore, the calculation of the average values of the functions in Eq. (17) may not be straightforward in practice.

C. Analysis of Condition $(\mathbf{n}\cdot\mathbf{s}) > 0$

In the special case when the sun vector is directed along the spin axis (i.e., when the solar aspect angle γ is either 0 or 180 deg), Eq. (15) shows that $(\mathbf{n}\cdot\mathbf{s}) = \pm\sin\mu$ remains constant. The condition $(\mathbf{n}\cdot\mathbf{s}) > 0$ is satisfied throughout the spin period if μ is positive (negative) when $\gamma = 0$ (180 deg). Another special case occurs when μ reaches its extremes of ± 90 deg, which represent a spacecraft top/bottom surface normal to the spin axis. In this case, Eq. (15) produces $(\mathbf{n}\cdot\mathbf{s}) = \pm\cos\gamma$, which again remains constant. The condition $(\mathbf{n}\cdot\mathbf{s}) > 0$ is satisfied throughout the spin period provided that the sun angle γ lies in the first/second quadrant, respectively. Figure 4 provides a visualization of these two special cases that represent the borders of the geometrically relevant domain within the γ–μ plane.

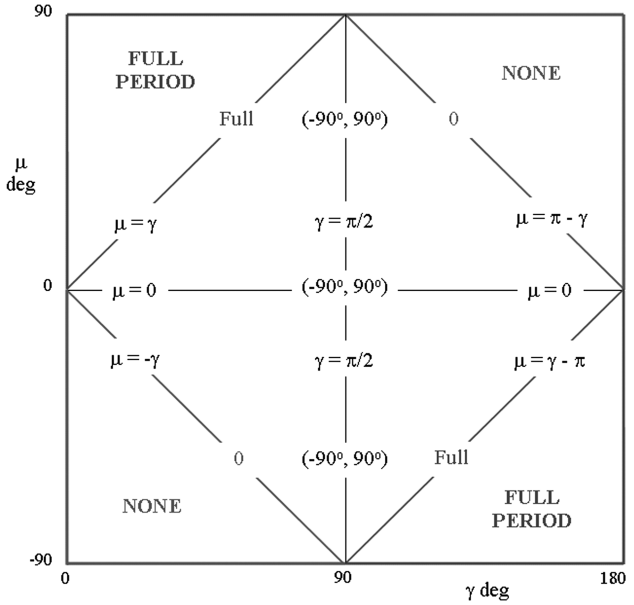

Fig. 4 Regions in the γ–μ plane with intervals in which $(\mathbf{n}\cdot\mathbf{s}) > 0$.

In general, the condition $(\mathbf{n}\cdot\mathbf{s}) > 0$ can be formulated as

$$\cos\tilde{\psi} > -g \tag{18}$$

where $g = \tan\mu/\tan\gamma$ [see Eq. (15)]. This condition is satisfied over the interval $|\tilde{\psi}| < \arccos(-g)$, which is meaningful as long as $|g| < 1$. The special case $\mu = 0$ represents a surface element parallel to the spin axis. In this case, we have $g = 0$ and the condition in Eq. (18) is satisfied over the interval $|\tilde{\psi}| \le 90$ deg for any value of the sun angle. The same result $|\tilde{\psi}| \le 90$ deg is obtained when $\gamma = 90$ deg, regardless of the value of the angle μ. Another interesting special case is $\mu = \gamma$, when g equals 1. This characterizes the boundary between $(\mathbf{n}\cdot\mathbf{s}) > 0$ throughout the *full* spin revolution and $(\mathbf{n}\cdot\mathbf{s}) > 0$ during only *part* of the spin period. In this case, Eq. (18) gives $\cos\tilde{\psi} = -1$ and the sun shines on the surface area throughout the spin period, except at $\tilde{\psi} = 180$ deg when the solar radiation is parallel to the surface area (Figs. 2 and 3). When γ lies in the first quadrant and $\mu > \gamma$, we find $g > 1$ and the condition of Eq. (18) is satisfied for any $\tilde{\psi}$ and the surface is sunlit throughout the spin period. The same is true when γ lies in the second quadrant and $\mu < \gamma - 180$ deg. In the cases $\mu = -\gamma$ and $\mu = 180$ deg $-\gamma$, we find g equals -1 and $(\mathbf{n}\cdot\mathbf{s}) < 0$ throughout the spin revolution, except at $\tilde{\psi} = 0$ when $(\mathbf{n}\cdot\mathbf{s}) = 0$. Other cases within the γ–μ plane can readily be interpreted with the help of Fig. 4.

In practical applications, the spacecraft consists of a number of surface elements A_i with individual normals $\mathbf{n}_i = (n_{ix}, n_{iy}, n_{iz})^T$ within the spacecraft frame. Each of these elements has its own $\mathbf{f}_{ai}$, $\mathbf{f}_{di}$, and $\mathbf{f}_{si}$ defined by Eq. (11), with $\mathbf{n}_i$ instead of $\mathbf{n}$, and its own functions $f_{kx,i}(\tilde{\psi})$, $f_{ky,i}(\tilde{\psi})$, and $f_{kz,i}(\tilde{\psi})$, with $k = a, d, s$, as defined in Eq. (16). Obviously, the condition $(\mathbf{n}_i\cdot\mathbf{s}) > 0$ of Eq. (10) must be evaluated for each of the surface elements individually. For a box-shaped spacecraft with four identical side-surface elements, the interval during the spin revolution when $(\mathbf{n}_i\cdot\mathbf{s}) > 0$ differs for each of these surfaces. It can be shown by geometrical arguments that the effective solar radiation force (after averaging over a spin period) will be identical for these four surface elements.

IV. Solar Radiation Torque Model

A. Calculation of Torque Components

The force $\mathbf{F}$ induced by solar radiation pressure on an arbitrary spacecraft element A acts at the center of pressure c_p of A (Fig. 3). Because the reflecting properties of the surface element A are assumed to be homogeneous, the point c_p coincides with the

geometrical center of A. The distance of c_p from the spacecraft center of mass c_m is denoted by the vector $\mathbf{r}$ and is known as the center-of-pressure offset. Obviously, $\mathbf{r}$ represents the lever arm of the solar radiation torque $\mathbf{T} = \mathbf{r} \times \mathbf{F}$ with respect to the spacecraft center of mass c_m.

The lever arm $\mathbf{r}$ has components $(r_x, r_y, r_z)^T$ within the spacecraft frame and can be expressed in terms of its right ascension and declination angles τ and χ (Fig. 3):

$$\mathbf{r} = r\cos\chi\cos\tau\,\mathbf{x} + r\cos\chi\sin\tau\,\mathbf{y} + r\sin\chi\,\mathbf{z} \tag{19}$$

We transform the instantaneous lever arm $\mathbf{r}$ to the sun-spin-axis frame (Fig. 2) in the same way as was done for the normal $\mathbf{n}$ to the surface element in Eqs. (12) and (13):

$$\mathbf{r}(\hat{\psi}) = r\cos\chi\cos\hat{\psi}\,\mathbf{x}_s + r\cos\chi\sin\hat{\psi}\,\mathbf{y}_s + r\sin\chi\,\mathbf{z}_s \tag{20}$$

The torque vector $\mathbf{T}$ must now be evaluated in its components in the sun-spin-axis reference frame. The cross products of Eqs. (16) and (20) are needed for building the torque vector of an individual surface area.

$$\mathbf{t}_a = \mathbf{r}(\hat{\psi}) \times \mathbf{f}_a(\tilde{\psi}) = r f_{az}(\tilde{\psi})\cos\chi\sin\hat{\psi}\,\mathbf{x}_s + r\{f_{ax}(\tilde{\psi})\sin\chi - f_{az}(\tilde{\psi})\cos\chi\cos\hat{\psi}\}\mathbf{y}_s - r f_{ax}(\tilde{\psi})\cos\chi\sin\hat{\psi}\,\mathbf{z}_s \tag{21a}$$

$$\mathbf{t}_d = \mathbf{r}(\hat{\psi}) \times \mathbf{f}_d(\tilde{\psi}) = r\{f_{dz}(\tilde{\psi})\cos\chi\sin\hat{\psi} - f_{dy}(\tilde{\psi})\sin\chi\}\mathbf{x}_s + r\{f_{dx}(\tilde{\psi})\sin\chi - f_{dz}(\tilde{\psi})\cos\chi\cos\hat{\psi}\}\mathbf{y}_s + r\cos\chi\{f_{dy}(\tilde{\psi})\cos\hat{\psi} - f_{dx}(\tilde{\psi})\sin\hat{\psi}\}\mathbf{z}_s \tag{21b}$$

$$\mathbf{t}_s = \mathbf{r}(\hat{\psi}) \times \mathbf{f}_s(\tilde{\psi}) = r\{f_{sz}(\tilde{\psi})\cos\chi\sin\hat{\psi} - f_{sy}(\tilde{\psi})\sin\chi\}\mathbf{x}_s + r\{f_{sx}(\tilde{\psi})\sin\chi - f_{sz}(\tilde{\psi})\cos\chi\cos\hat{\psi}\}\mathbf{y}_s + r\cos\chi\{f_{sy}(\tilde{\psi})\cos\hat{\psi} - f_{sx}(\tilde{\psi})\sin\hat{\psi}\}\mathbf{z}_s \tag{21c}$$

B. Total Average Force and Torque Expressions

The resulting total torque acting on the spacecraft is given by the sum of all individual solar radiation torques produced by the forces $\mathbf{F}_i$ on the corresponding elements A_i:

$$\mathbf{T} = \Sigma_i\{\mathbf{T}_i\} = \Sigma_i\{\mathbf{r}_i \times \mathbf{F}_i\} \tag{22}$$

The generic form of the force given in Eq. (10) must be evaluated for each surface element A_i. The cross product of the lever arm $\mathbf{r}_i$ (of the elements A_i) and the solar radiation forces $\mathbf{F}_i$ in Eq. (21) need to be calculated for each surface element individually before they are summed. The total average solar radiation torque over a spacecraft spin revolution equals the sum of the averaged contributions from all relevant surface elements A_i. This procedure leads to the effective torque in components along the quasi-inertial sun-spin-axis frame.

Each of the surface elements has its own normal $\mathbf{n}_i$ that determines the individual spin-angle range $|\tilde{\psi}_i| < \arccos(-g_i)$ with $g_i = \tan\mu_i/\tan\gamma$ [Eq. (18)], during which the condition $(\mathbf{n}_i \cdot \mathbf{s}) > 0$ is satisfied. Thus, the total average solar radiation force and torque can be written as

$$\langle\mathbf{F}\rangle = \frac{1}{2\pi}\sum_i \int_{(\mathbf{n}_i\cdot\mathbf{s})>0} \mathbf{F}_i(\tilde{\psi}_i)\,d\tilde{\psi}_i \tag{23a}$$

$$\langle\mathbf{T}\rangle = \frac{1}{2\pi}\sum_i \int_{(\mathbf{n}_i\cdot\mathbf{s})>0} \{\mathbf{r}_i \times \mathbf{F}_i(\tilde{\psi}_i)\}\,d\tilde{\psi}_i \tag{23b}$$

The notation $\langle\ldots\rangle$ designates the averaging operation that is shown in explicit form in Eq. (23). In general, it is not allowed to take $\mathbf{r}_i$ outside the integral, because both $\mathbf{r}_i$ and $\mathbf{F}_i$ are periodic functions of the spin-phase angle $\tilde{\psi}_i$ within the sun-spin-axis frame.

The total average solar radiation force and torque expressions of Eq. (23) can be reduced using Eq. (10):

$$\langle\mathbf{F}\rangle = -P\sum_i \{(1-\rho)\langle\mathbf{f}_{ai}\rangle + \sigma\langle\mathbf{f}_{di}\rangle + 2\rho\langle\mathbf{f}_{si}\rangle\} \tag{24a}$$

$$\langle\mathbf{T}\rangle = -P\sum_i \{(1-\rho)\langle\mathbf{t}_{ai}\rangle + \sigma\langle\mathbf{t}_{di}\rangle + 2\rho\langle\mathbf{t}_{si}\rangle\} \tag{24b}$$

The calculation of the average solar radiation force over the relevant part of the spin revolution involves the evaluation of the integrals over the force expression defined in Eq. (11):

$$\langle\mathbf{f}_{ai}\rangle = \langle(\mathbf{n}_i\cdot\mathbf{s})\mathbf{s}\rangle = \frac{1}{2\pi}\int_{(\mathbf{n}_i\cdot\mathbf{s})>0} \mathbf{f}_{ai}(\tilde{\psi}_i)\,d\tilde{\psi}_i \tag{25a}$$

$$\langle\mathbf{f}_{di}\rangle = \langle(\mathbf{n}_i\cdot\mathbf{s})\mathbf{n}_i\rangle = \frac{1}{2\pi}\int_{(\mathbf{n}_i\cdot\mathbf{s})>0} \mathbf{f}_{di}(\tilde{\psi}_i)\,d\tilde{\psi}_i \tag{25b}$$

$$\langle\mathbf{f}_{si}\rangle = \langle(\mathbf{n}_i\cdot\mathbf{s})^2\mathbf{n}_i\rangle = \frac{1}{2\pi}\int_{(\mathbf{n}_i\cdot\mathbf{s})>0} \mathbf{f}_{si}(\tilde{\psi}_i)\,d\tilde{\psi}_i \tag{25c}$$

The integrands were defined in Eq. (16) and must be evaluated for each surface element A_i individually.

The calculation of the average solar radiation torque involves the following integrals:

$$\langle\mathbf{t}_{ai}\rangle = \langle(\mathbf{n}_i\cdot\mathbf{s})(\mathbf{r}_i\times\mathbf{s})\rangle = \frac{1}{2\pi}\int_{(\mathbf{n}_i\cdot\mathbf{s})>0} \{\mathbf{r}_i(\hat{\psi}_i)\times\mathbf{f}_{ai}(\tilde{\psi}_i)\}\,d\tilde{\psi}_i \tag{26a}$$

$$\langle\mathbf{t}_{di}\rangle = \langle(\mathbf{n}_i\cdot\mathbf{s})(\mathbf{r}_i\times\mathbf{n}_i)\rangle = \frac{1}{2\pi}\int_{(\mathbf{n}_i\cdot\mathbf{s})>0} \{\mathbf{r}_i(\hat{\psi}_i)\times\mathbf{f}_{di}(\tilde{\psi}_i)\}\,d\tilde{\psi}_i \tag{26b}$$

$$\langle\mathbf{t}_{si}\rangle = \langle(\mathbf{n}_i\cdot\mathbf{s})^2(\mathbf{r}_i\times\mathbf{n}_i)\rangle = \frac{1}{2\pi}\int_{(\mathbf{n}_i\cdot\mathbf{s})>0} \{\mathbf{r}_i(\hat{\psi}_i)\times\mathbf{f}_{si}(\tilde{\psi}_i)\}\,d\tilde{\psi}_i \tag{26c}$$

The integrands of Eq. (26) are defined in Eq. (21) and need to be evaluated for each individual surface element. These results are valid for arbitrary spacecraft configurations and will be illustrated for a few special cases next.

V. Examples of Averaged Forces and Torques

A. Surface Element Normal to the Spin Axis

The most straightforward illustration of the preceding model is provided by a surface area A that is oriented normal to the spin axis (e.g., a spacecraft top surface or a flat solar sail with an arbitrary offset between its center of pressure and the satellite's center of mass). To evaluate the effects of small deviations in the nominal orientation of the surface area, we take the normal $\mathbf{n}$ to the surface area to be slightly misaligned from its ideal direction (i.e., $\mu = \pi/2 - \varepsilon$) with an arbitrary phase angle ν. The expression for the normal vector $\mathbf{n}$ to the single surface element A follows from Eq. (13):

$$\mathbf{n}(\tilde{\psi}) = \mathbf{z}_s + \varepsilon\cos\tilde{\psi}\,\mathbf{x}_s + \varepsilon\sin\tilde{\psi}\,\mathbf{y}_s + \mathcal{O}(\varepsilon^2) \tag{27}$$

The first-order approximation of the inner product $(\mathbf{n}\cdot\mathbf{s})$ in Eq. (15) is

$$\{\mathbf{n}(\tilde{\psi})\cdot\mathbf{s}\} = \cos\gamma + \varepsilon\sin\gamma\cos\tilde{\psi} + \mathcal{O}(\varepsilon^2) \tag{28}$$

When substituting $\mu = \pi/2 - \varepsilon$ into Eq. (18), we find that the condition $(\mathbf{n}\cdot\mathbf{s}) > 0$ or $\cos\tilde{\psi} > -g$ will be satisfied for any value of $\tilde{\psi}$, based on the fact that $g \approx 1/(\varepsilon\tan\gamma) > 1$. An exception occurs when $\gamma > \pi/2 - \varepsilon$. This implies that the sun would be closer to the surface element than the value of the misalignment angle ε, which we exclude here.

After performing the averaging operation over the spin period, the ε term on the right-hand side of Eq. (28) vanishes and the leading term leads to a constant contribution:

$$\langle\{\mathbf{n}(\tilde{\psi})\cdot\mathbf{s}\}\rangle = \frac{1}{2\pi}\int_{(\mathbf{n}\cdot\mathbf{s})>0}\{\mathbf{n}(\tilde{\psi})\cdot\mathbf{s}\}d\tilde{\psi} = \cos\gamma + \mathcal{O}(\varepsilon^2) \quad (29)$$

The force terms of Eq. (16) can be simplified by substituting $\mu = \pi/2 - \varepsilon$:

$$f_{ax} = \sin\gamma\cos\gamma + \varepsilon\sin^2\gamma\cos\tilde{\psi} + \mathcal{O}(\varepsilon^2); \qquad f_{ay} = 0$$
$$f_{az} = \cos^2\gamma + \tfrac{1}{2}\varepsilon\sin(2\gamma)\cos\tilde{\psi} + \mathcal{O}(\varepsilon^2) \quad (30a)$$

$$f_{dx} = \varepsilon\cos\gamma\cos\tilde{\psi} + \mathcal{O}(\varepsilon^2); \qquad f_{dy} = \varepsilon\cos\gamma\sin\tilde{\psi} + \mathcal{O}(\varepsilon^2)$$
$$f_{dz} = \cos\gamma + \varepsilon\sin\gamma\cos\tilde{\psi} + \mathcal{O}(\varepsilon^2) \quad (30b)$$

$$f_{sx} = \varepsilon\cos^2\gamma\cos\tilde{\psi} + \mathcal{O}(\varepsilon^2); \qquad f_{sy} = \varepsilon\cos^2\gamma\sin\tilde{\psi} + \mathcal{O}(\varepsilon^2)$$
$$f_{sz} = \cos^2\gamma + \varepsilon\sin(2\gamma)\cos\tilde{\psi} + \mathcal{O}(\varepsilon^2) \quad (30c)$$

After averaging these expressions over the spin period, we find:

$$\langle\mathbf{f}_a\rangle = \sin\gamma\cos\gamma\,\mathbf{x}_s + \cos^2\gamma\,\mathbf{z}_s + \mathcal{O}(\varepsilon^2) \quad (31a)$$

$$\langle\mathbf{f}_d\rangle = \cos\gamma\,\mathbf{z}_s + \mathcal{O}(\varepsilon^2) \quad (31b)$$

$$\langle\mathbf{f}_s\rangle = \cos^2\gamma\,\mathbf{z}_s + \mathcal{O}(\varepsilon^2) \quad (31c)$$

Finally, after averaging the solar radiation force over a full spin revolution, we find that the resulting averaged force vector lies within the sun-spin-axis plane:

$$\langle\mathbf{F}\rangle = -P\cos\gamma\{[(1-\rho)\sin\gamma]\mathbf{x}_s + [(1+\rho)\cos\gamma + \sigma]\mathbf{z}_s\} + \mathcal{O}(\varepsilon^2) \quad (32)$$

This result shows that small errors in the orientation of the surface elements have a negligible second-order effect on the resulting average solar radiation force.

The cross products that appear in the integrands of the torque expressions of Eq. (26) were given in explicit forms in Eq. (21). After substituting $\mu = \pi/2 - \varepsilon$ and averaging over the spin period, we find

$$\langle\mathbf{t}_a\rangle = \tfrac{1}{2}r\sin\chi\sin(2\gamma)\mathbf{y}_s + \tfrac{1}{2}\varepsilon r\cos\chi\sin\gamma\{\cos\gamma\sin(\tau-\nu)\mathbf{x}_s$$
$$-\cos\gamma\cos(\tau-\nu)\mathbf{y}_s - \sin\gamma\sin(\tau-\nu)\mathbf{z}_s\} + \mathcal{O}(\varepsilon^2) \quad (33a)$$

$$\langle\mathbf{t}_d\rangle = \tfrac{1}{2}\varepsilon r\cos\chi\{\sin\gamma\sin(\tau-\nu)\mathbf{x}_s - \sin\gamma\cos(\tau-\nu)\mathbf{y}_s$$
$$-2\cos\gamma\sin(\tau-\nu)\mathbf{z}_s\} + \mathcal{O}(\varepsilon^2) \quad (33b)$$

$$\langle\mathbf{t}_s\rangle = \varepsilon r\cos\chi\cos\gamma\{\sin\gamma\sin(\tau-\nu)\mathbf{x}_s - \sin\gamma\cos(\tau-\nu)\mathbf{y}_s$$
$$-\cos\gamma\sin(\tau-\nu)\mathbf{z}_s\} + \mathcal{O}(\varepsilon^2) \quad (33c)$$

These results indicate that the misalignment angle ε may, in general, cause windmill-type torque effects about the $\mathbf{z}_s$ and $\mathbf{x}_s$ axes. However, in the special case when $\tau = \nu$, the normal $\mathbf{n}$ to the surface element and the torque lever arm $\mathbf{r}$ lie in the same plane (Fig. 3) and we obtain the simplified torque expressions (up to first-order ε terms):

$$\langle\mathbf{t}_a\rangle \approx \tfrac{1}{2}r\sin\chi\sin(2\gamma)\mathbf{y}_s - \tfrac{1}{4}\varepsilon r\cos\chi\sin(2\gamma)\mathbf{y}_s \quad (34a)$$

$$\langle\mathbf{t}_d\rangle \approx -\tfrac{1}{2}\varepsilon r\cos\chi\sin\gamma\,\mathbf{y}_s \quad (34b)$$

$$\langle\mathbf{t}_s\rangle \approx -\tfrac{1}{2}\varepsilon r\cos\chi\sin(2\gamma)\mathbf{y}_s \quad (34c)$$

The contribution of the constant z_s force component in Eq. (31) has no effect, because the circulating in-plane component of the lever arm vanishes after averaging. The resulting torque vector in Eq. (24b) will be directed along the y_s axis (i.e., normal to the sun-spin-axis plane). Its leading term originates from the absorptive force component along the x_s axis:

$$\langle\mathbf{T}\rangle \approx -\tfrac{1}{2}P(1-\rho)r\sin\chi\sin(2\gamma)\mathbf{y}_s \quad (35)$$

It can be seen that the leading term of $\langle\mathbf{T}\rangle$ in Eq. (35) equals $\langle\mathbf{r}\rangle\times\langle\mathbf{F}\rangle$, with $\langle\mathbf{r}\rangle = r\sin\chi\mathbf{z}_s$ from Eq. (20) and $\langle\mathbf{F}\rangle$ in Eq. (32). When the center-of-pressure offset lies within the spacecraft x–y plane (i.e., $\chi = 0$), the leading term of the average torque vanishes (in the present example) due to the circulating lever arm. However, all of the first-order contributions listed in Eq. (34) would remain. On the other hand, when the center-of-pressure offset is along the spin axis (i.e., $\chi = 90$ deg), a nonzero leading-term torque will be generated (unless the solar aspect angle γ is 0 or 90 deg). This torque would affect the long-term evolution of the spacecraft spin-axis orientation.

B. Surface Element Parallel to the Spin Axis

The second special case represents a surface element A oriented parallel to the spin axis (for instance, a side panel of a spinning spacecraft). In this case, the declination angle μ of the normal vector $\mathbf{n}$ is nominally zero. To also assess the effect of a small error in the alignment of the surface (or in the spin-axis orientation), we take $\mu = \varepsilon$. When including only first-order ε terms, the expression for the normal vector $\mathbf{n}$ from Eq. (13) takes the form

$$\mathbf{n}(\tilde{\psi}) = \cos\tilde{\psi}\,\mathbf{x}_s + \sin\tilde{\psi}\,\mathbf{y}_s + \varepsilon\,\mathbf{z}_s + \mathcal{O}(\varepsilon^2) \quad (36)$$

Equation (15) now becomes

$$\mathbf{n}(\tilde{\psi})\cdot\mathbf{s} = \sin\gamma\cos\tilde{\psi} + \varepsilon\cos\gamma + \mathcal{O}(\varepsilon^2) \quad (37)$$

The solutions of the equation $\mathbf{n}(\tilde{\psi})\cdot\mathbf{s} = 0$ are $\tilde{\psi}_1 \approx -\pi/2 - \varepsilon/\tan\gamma$ and $\tilde{\psi}_2 \approx \pi/2 + \varepsilon/\tan\gamma$ in first-order approximation. Furthermore, it can be seen that $\mathbf{n}(\tilde{\psi})\cdot\mathbf{s}$ is positive over the interval from $\tilde{\psi}_1$ to $\tilde{\psi}_2$ for any solar aspect angle γ away from the spin axis, and so the first-order approximation of the average value of $\mathbf{n}(\tilde{\psi})\cdot\mathbf{s}$ over the relevant interval is

$$\langle\{\mathbf{n}(\tilde{\psi})\cdot\mathbf{s}\}\rangle = \frac{1}{2\pi}\int_{\tilde{\psi}_1}^{\tilde{\psi}_2}\{\mathbf{n}(\tilde{\psi})\cdot\mathbf{s}\}d\tilde{\psi} \approx (1/\pi)\sin\gamma + \frac{1}{2}\varepsilon\cos\gamma \quad (38)$$

The force terms of Eq. (16) can be simplified when substituting $\mu = \varepsilon$. Their first-order approximations are

$$f_{ax} \approx \sin^2\gamma\cos\tilde{\psi} + \tfrac{1}{2}\varepsilon\sin(2\gamma); \qquad f_{ay} \approx 0$$
$$f_{az} \approx \tfrac{1}{2}\sin(2\gamma)\cos\tilde{\psi} + \varepsilon\cos^2\gamma \quad (39a)$$

$$f_{dx} \approx \sin\gamma\cos^2\tilde{\psi} + \varepsilon\cos\gamma\cos\tilde{\psi}$$
$$f_{dy} \approx \tfrac{1}{2}\sin\gamma\sin(2\tilde{\psi}) + \varepsilon\cos\gamma\sin\tilde{\psi}; \qquad f_{dz} \approx \varepsilon\sin\gamma\cos\tilde{\psi} \quad (39b)$$

$$f_{sx} \approx \sin^2\gamma\cos^3\tilde{\psi} + \varepsilon\sin(2\gamma)\cos^2\tilde{\psi}$$
$$f_{sy} \approx \sin^2\gamma\sin\tilde{\psi}\cos^2\tilde{\psi} + \tfrac{1}{2}\varepsilon\sin(2\gamma)\sin(2\tilde{\psi}) \quad (39c)$$
$$f_{sz} \approx \varepsilon\sin^2\gamma\cos^2\tilde{\psi}$$

The time-varying geometry of the surface element relative to the sun causes the leading terms to be functions of $\tilde{\psi}$ in the present case. After performing the averaging operation on these expressions over the interval from $\tilde{\psi}_1$ to $\tilde{\psi}_2$, we find the first-order results:

$$\langle\mathbf{f}_a\rangle \approx \{(1/\pi)\sin\gamma + \tfrac{1}{2}\varepsilon\cos\gamma\}\{\sin\gamma\,\mathbf{x}_s + \cos\gamma\,\mathbf{z}_s\} \quad (40a)$$

$$\langle\mathbf{f}_d\rangle \approx \tfrac{1}{4}\sin\gamma\,\mathbf{x}_s + (\varepsilon/\pi)\{\tfrac{3}{2}\cos\gamma\,\mathbf{x}_s + \sin\gamma\,\mathbf{z}_s\} \quad (40b)$$

$$\langle\mathbf{f}_s\rangle \approx 2/(3\pi)\sin^2\gamma\,\mathbf{x}_s + \tfrac{1}{4}\varepsilon\sin\gamma\{2\cos\gamma\,\mathbf{x}_s + \sin\gamma\,\mathbf{z}_s\} \quad (40c)$$

We find the following final expression for the force (including the first-order misalignment terms):

$$\langle \mathbf{F} \rangle \approx -(P/\pi)\sin\gamma\{[(1+\rho/3)\sin\gamma + \pi\sigma/4]\mathbf{x}_s + [(1-\rho)\cos\gamma]\mathbf{z}_s\} - \tfrac{1}{2}\varepsilon P\{\cos\gamma[(1+\rho)\sin\gamma + 3\sigma/\pi]\mathbf{x}_s + [\rho + (1-2\rho)\cos^2\gamma + (\sigma/\pi)\sin\gamma]\mathbf{z}_s\} \quad (41)$$

This result shows that the leading and first-order misalignment terms of the average solar radiation force are acting within the sun-spin-axis plane.

When substituting the force terms of Eq. (39) and averaging the expressions of Eq. (21), as illustrated in Eq. (26), we find the following results for the leading torque terms:

$$\langle \mathbf{t}_a \rangle \approx \tfrac{1}{4} r\sin\gamma\{-\cos\gamma\cos\chi\sin(\nu-\tau)\mathbf{x}_s + [(4/\pi)\sin\chi\sin\gamma - \cos\chi\cos\gamma\cos(\nu-\tau)]\mathbf{y}_s + \cos\chi\sin\gamma\sin(\nu-\tau)\mathbf{z}_s\} \quad (42a)$$

$$\langle \mathbf{t}_d \rangle \approx \tfrac{1}{4} r\sin\gamma\{\sin\chi\,\mathbf{y}_s + (4/\pi)\cos\chi\sin(\nu-\tau)\mathbf{z}_s\} \quad (42b)$$

$$\langle \mathbf{t}_s \rangle \approx 2/(3\pi) r\sin^2\gamma\{\sin\chi\,\mathbf{y}_s + \tfrac{1}{4}\cos\chi\sin(\nu-\tau)\mathbf{z}_s\} \quad (42c)$$

The simplifying assumption that the orientation of the normal vector of the surface element and the lever-arm vector lie in the same plane will now also be adopted in the present example. Therefore, the normal and the lever arm will have the same spin-phase angle and the angles ν and τ become equal. The leading term of the averaged torque takes now the form

$$\langle \mathbf{T} \rangle \approx -(P/\pi) r\sin\gamma\{\sin\chi[(1+\rho/3)\sin\gamma + \pi\sigma/4] - (\pi/4)(1-\rho)\cos\chi\cos\gamma\}\mathbf{y}_s \quad (43)$$

When comparing the results of Eqs. (41) and (43), we find that the leading torque term $\langle \mathbf{T} \rangle \neq \langle \mathbf{r} \rangle \times \langle \mathbf{F} \rangle$ in this case.

For completeness, we also provide the first-order averaged-torque terms for the special case when ν and τ are equal:

$$\langle \mathbf{t}_a \rangle_{\text{first order}} = \tfrac{1}{2}\varepsilon r\cos\gamma\{\sin\chi\sin\gamma - (3/\pi)\cos\chi\cos\gamma\}\mathbf{y}_s \quad (44a)$$

$$\langle \mathbf{t}_d \rangle_{\text{first order}} \approx \tfrac{1}{4}\varepsilon r\{(6/\pi)\sin\chi\cos\gamma - \cos\chi\sin\gamma\}\mathbf{y}_s \quad (44b)$$

$$\langle \mathbf{t}_s \rangle_{\text{first order}} \approx \tfrac{1}{2}\varepsilon r\sin\gamma\{\sin\chi\cos\gamma - 4/(3\pi)\cos\chi\sin\gamma\}\mathbf{y}_s \quad (44c)$$

As in the previous example, the resulting averaged-torque points in the direction normal to the sun-spin-axis plane.

C. Generic Force and Torque Expressions

The force and torque results established for the two preceding special cases are useful for evaluating the solar radiation effects on arbitrary spacecraft configurations. This is done by identifying the relevant surface areas with their specific material properties and simply adding the individual averaged contributions. For instance, when studying a spacecraft of rectangular shape with four side surfaces with identical material properties, the contributions of each surface will be equal (after averaging over a spin period), and so the force and torque results in Eqs. (32), (35), (41), and (43) need only to be multiplied by a factor of 4.

The torque results for the two examples presented may be written in the generic form:

$$\langle \mathbf{F} \rangle = -P\{f_1\mathbf{x}_s + f_2\mathbf{z}_s\}; \qquad \langle \mathbf{T} \rangle = -Pr\{g_1\sin\chi - g_2\cos\chi\}\mathbf{y}_s \quad (45)$$

The lever arm r represents the offset of the center of pressure with respect to the center of mass and has components $r_z = r\sin\chi$ along the spin axis and $r_p = r\cos\chi$ within the plane normal to the spin axis. The force and torque terms f_1, f_2, g_1, and g_2 contain the material parameters of the spacecraft surfaces, but they also depend on the solar aspect angle, as summarized in Table 1. Although the g_1 torque terms in the two cases of Table 1 are identical to the associated f_1 of the force expression, this correspondence may not be true in general.

A final assumption may be introduced to simplify the torque expression. When the satellite surfaces are assumed to be essentially specularly reflecting (i.e., $\rho \approx 1$ and $\sigma \approx 0$), the only remaining torque term is produced by the side surfaces (Table 1):

$$\langle \mathbf{T} \rangle = -Prg_1\sin\chi\,\mathbf{y}_s = -4Pr_z\sin^2\gamma/(3\pi)\mathbf{y}_s \quad (46)$$

The sign of $\langle \mathbf{T} \rangle$ is determined by the sign of the center-of-pressure offset along the spin axis (i.e., r_z).

VI. Long-Term Evolution of Spin-Axis Pointing

A. Precession of Angular Momentum

The effect of the average torque on the attitude motion follows from Newton's second law for rotating rigid bodies, and so the torque vector equals the rate of change of the angular momentum vector. Because the SRP torque is relatively small, the change in the angular momentum vector over a spin period may be considered infinitesimal. It was found in Eqs. (45) and (46) that the average SRP torque acts in a direction perpendicular to the instantaneous angular momentum vector $\mathbf{H}$ so that only the direction of $\mathbf{H}$ will be affected. The infinitesimal change $\Delta\mathbf{H}$ in the angular momentum vector over the spin period Δt can be written as follows [14]:

$$\mathbf{T} = \mathrm{d}\mathbf{H}/\mathrm{dt} \rightarrow \Delta\mathbf{H} \approx \langle \mathbf{T} \rangle \Delta t \quad (47)$$

The change $\Delta\mathbf{H}$ is normal to the vector $\mathbf{H}$ and points along the vector $\langle \mathbf{T} \rangle$, which acts in the $-y_s$ direction of the quasi-inertial sun-spin-axis frame [when assuming $r_z > 0$ in Eq. (46)]. The angle $\Delta\vartheta$ over which the angular momentum vector moves during one spin period can be calculated as follows (Wertz [15], Eq. 19.61):

$$\Delta\vartheta \approx |\Delta\mathbf{H}|/|\mathbf{H}| = T\Delta t/(I_z\omega)\ \text{[rad]} \quad (48)$$

The quasi-inertial (x_s, y_s, z_s) reference frame in Fig. 2 is defined by the instantaneous directions of the spacecraft spin axis and the sun vector. This frame is subject to a gradual drift under the combined motion of the sun vector $\mathbf{s}$ and the precession $\mathbf{w}$ induced by the SRP torque. To be able to apply Newton's law, this frame must be redefined after every spin period and be considered constant during the spin revolution.

The direction of the torque precession $\mathbf{w}$ is normal to the instantaneous $\mathbf{H}$ and the $\langle \mathbf{T} \rangle$ vectors. For $r_z > 0$, the torque points along the negative y_s axis and the vector $\mathbf{w}$ will be along the positive x_s axis. The precession magnitude follows from Eq. (48):

$$\langle \mathbf{T} \rangle = \mathbf{w} \times \mathbf{H} \rightarrow w = |\mathbf{w}| \approx \Delta\vartheta/\Delta t = T/(I_z\omega)\ \text{[rad/s]} \quad (49)$$

Table 1 Leading terms of the force and torque results

	Surface element normal to the spin axis	
Force components	$f_1 = (1-\rho)\sin\gamma\cos\gamma$	$f_2 = \cos\gamma[(1+\rho)\cos\gamma + \sigma]$
Torque components	$g_1 = (1-\rho)\sin\gamma\cos\gamma$	$g_2 = 0$
	Surface element parallel to the spin axis	
Force components	$f_1 = \sin\gamma[(1+\rho/3)(\sin\gamma)/\pi + \sigma/4]$	$f_2 = (1-\rho)[\sin\gamma\cos\gamma]/\pi$
Torque components	$g_1 = \sin\gamma[(1+\rho/3)(\sin\gamma)/\pi + \sigma/4]$	$g_2 = \frac{1}{4}(1-\rho)\sin\gamma\cos\gamma$

The orientation of the satellite spin axis itself is affected by the change in the angular momentum vector in a complicated manner. It is well known that for a spacecraft spinning about its axis of maximum moment of inertia, the spin axis tends to align itself with the direction of the angular momentum vector, which corresponds to the minimum-energy state. However, for a spacecraft that spins about its minimum axis of inertia, an active nutation damping device must be employed. Nutational effects amount to no more than minor deviations from the long-term trend presented here and may be ignored in the present analysis.

B. Model for Spin-Axis Motion

The long-term evolution of the spacecraft spin axis $\mathbf{z}(t)$ under the precession rate $\mathbf{w}(t)$ induced by the SRP torque follows the motion of the angular momentum vector and can be described by

$$\dot{\mathbf{z}}(t) = \mathbf{w} \times \mathbf{z} = w\{\mathbf{x}_s \times \mathbf{z}\} \tag{50}$$

The vector $\dot{\mathbf{z}}$ points in the direction of $T = \langle \mathbf{T} \rangle$, which is along $-y_s$ for $r_z > 0$. When using the definition of the x_s axis in Eq. (4), it is easy to eliminate the $\mathbf{x}_s$ vector in Eq. (50) in favor of the sun vector:

$$\dot{\mathbf{z}}(t) = w\{\mathbf{s} \times \mathbf{z}\}/\sin\gamma \tag{51}$$

When substituting the results of Eqs. (46), (49), and (51), we obtain

$$\dot{\mathbf{z}}(t) = Q \sin\gamma\{\mathbf{s} \times \mathbf{z}\} \tag{52}$$

where $Q = 4Pr_z/(3\pi I_z\omega)$ [rad/s].

C. Approximate Solution

To construct an approximate solution of Eq. (52), we assume that the long-term variations in the spacecraft attitude remain small (say, less than 5 deg) so that the $\mathbf{z}$ vector in the right-hand side of Eq. (52) may be replaced by its initial value $\mathbf{z}_0 = \mathbf{z}(t = 0)$. Furthermore, the variations in the solar aspect angle will also be assumed to remain small. In practical applications, the most accurate results are obtained when taking the averaged (over the full year) solar aspect angle value γ_{avg} over the year (on the basis of the vector $\mathbf{z}_0$), rather than the initial sun angle γ_0. The sun vector $\mathbf{s}$ in Eq. (52) is now replaced by its inertial components as a function of the sun's longitude $\lambda_\odot(d) = \omega_\odot(d - d_\gamma)$ given in Eq. (2):

$$z_1'(d) \approx Q \sin\gamma_{\text{ave}}\{z_{30}\cos\varepsilon_\odot - z_{20}\sin\varepsilon_\odot\}\sin\lambda_\odot(d) \tag{53a}$$

$$z_2'(d) \approx Q \sin\gamma_{\text{ave}}\{z_{10}\sin\varepsilon_\odot \sin\lambda_\odot(d) - z_{30}\cos\lambda_\odot(d)\} \tag{53b}$$

$$z_3'(d) \approx Q \sin\gamma_{\text{ave}}\{z_{20}\cos\lambda_\odot(d) - z_{10}\cos\varepsilon_\odot \sin\lambda_\odot(d)\} \tag{53c}$$

The independent variable is expressed in days d relative to the vernal equinox. We evaluate the integrals with the help of Eqs. (2) and (3):

$$\int_{d_0}^{d} \cos\lambda_\odot(s)ds = S(d, d_0)/\omega_\odot \tag{54a}$$

where $S(d, d_0) = \sin\lambda_\odot(d) - \sin\lambda_\odot(d_0)$.

$$\int_{d_0}^{d} \sin\lambda_\odot(s)ds = -C(d, d_0)/\omega_\odot \tag{54b}$$

where $C(d, d_0) = \cos\lambda_\odot(d) - \cos\lambda_\odot(d_0)$.

The solutions of Eq. (53) are now

$$z_1(d, d_0) \approx z_{10} + W(z_{20}\sin\varepsilon_\odot - z_{30}\cos\varepsilon_\odot)C(d, d_0) \tag{55a}$$

$$z_2(d, d_0) \approx z_{20} - Wz_{10}\sin\varepsilon_\odot C(d, d_0) - Wz_{30}S(d, d_0) \tag{55b}$$

$$z_3(d, d_0) \approx z_{30} + Wz_{20}S(d, d_0) + Wz_{10}\cos\varepsilon_\odot C(d, d_0) \tag{55c}$$

The nondimensional parameter W equals $Q\sin\gamma_{\text{ave}}/\omega_\odot$ and is a relatively small quantity of the order of magnitude of 10^{-2}.

D. Spin Axis Normal to the Ecliptic

In the special case when the initial spin axis is pointing close to normal to the ecliptic plane, we have $\sin\gamma_0 \approx 1$ and, when assuming that the attitude excursions remain small, also $\sin\gamma_{\text{ave}} \approx 1$ and thus $W \approx Q/\omega_\odot$. When analyzing this case, it is most convenient to employ ξ, η, and ζ, describing the components of the attitude vector $\mathbf{z}$ within the ecliptic reference frame:

$$\begin{pmatrix} \xi \\ \eta \\ \zeta \end{pmatrix} = \begin{bmatrix} 1 & 0 & 0 \\ 0 & \cos\varepsilon_\odot & \sin\varepsilon_\odot \\ 0 & -\sin\varepsilon_\odot & \cos\varepsilon_\odot \end{bmatrix} \begin{pmatrix} z_1 \\ z_2 \\ z_3 \end{pmatrix} \tag{56}$$

The initial spin vector that is normal to the ecliptic is defined by $\xi_0 = \eta_0 = 0$ and $\zeta_0 = \pm 1$. When considering $\zeta_0 = 1$, the vector corresponds to $\mathbf{z}_0 = (0, -\sin\varepsilon_\odot, \cos\varepsilon_\odot)^T$ in the equatorial inertial frame [see also Eq. (7)]. After applying the transformation in Eq. (56), we find for the results of Eq. (55):

$$\xi(d, d_0) \approx -W\{\cos\lambda_\odot(d) - \cos\lambda_\odot(d_0)\} \tag{57a}$$

$$\eta(d, d_0) \approx -W\{\sin\lambda_\odot(d) - \sin\lambda_\odot(d_0)\} \tag{57b}$$

$$\zeta(d, d_0) \approx 1 \tag{57c}$$

The evolution of the spin-axis vector can be interpreted as the periodic circular motion of the projected $\mathbf{z}$ vector in the ecliptic plane as follows:

$$\{\xi(d) - Wc_0\}^2 + \{\eta(d) - Ws_0\}^2 \approx W^2 \tag{58}$$

with c_0 and s_0 denoting the cosine and sine of $\lambda_\odot(d_0)$, respectively.

For illustration, we take the starting date at the vernal equinox ($d_0 = d_\gamma$) so that $c_0 = 1$ and $s_0 = 0$, according to Eq. (3). The projected attitude vector describes a circle with its center on the ξ axis at the point $\xi_c = W$ and $\eta_c = 0$. The spin-axis attitude excursion will reach its maximum value $\xi_{\max}$ after half a year with

$$\xi_{\max} = 2\xi_c \approx 2W = 2Q/\omega_\odot \tag{59}$$

For different starting dates, it can easily be shown that the same maximum attitude excursion will be reached after a half-year interval as well.

VII. Practical Applications of Model

A. Maximum Spin-Axis Excursion

The application of the preceding model for the long-term attitude motion is illustrated for a satellite with its spin axis oriented close to the ecliptic pole direction. The CONTOUR deep space probe was designed to be left unattended during a number of hibernation periods with durations of up to 10 months [12]. Because of system-level design and operational considerations, it was attractive to have the spin axis pointing in a direction close to the ecliptic pole. This attitude orientation leads to relatively small variations in the spacecraft power and thermal conditions. It is crucial to have a good understanding of the maximum possible reach of the resulting attitude motion during the hibernation phases. The relevant design parameters of the CONTOUR spacecraft are listed in the second column of Table 2. The solar aspect angle γ is always close to 90 deg for an attitude-pointing orientation in the neighborhood of the ecliptic pole. On the basis of this condition, the general results of Table 1 indicate that the force and torque effects generated by the top and bottom surfaces may be neglected.

The adopted satellite configuration is approximately cylindrical with height $h = 1.75$ m and radius $r_{\text{cyl}} = 0.9$ m, and so the total cylindrical surface area is close to 10 m^2. The worst-case center-of-pressure offset along the spin axis is expected to be $r_z \approx 5$ cm. Because the objective is to arrive at a worst-case estimate for the attitude drift, conservative values are taken for the surface reflectivity parameter ($\rho \approx 1$), for the spin rate (15 rpm), for the spin moment of inertia (285 kg/m^2), and for the distance from the sun (1 AU).

Table 2 Overview of spacecraft parameters

Parameters	CONTOUR	Minisatellite
γ	$\approx$90 deg	$\approx$90 deg
h	1.75 m	0.8 m
A	$2\pi \times 1.75 \times 0.9$ m^2	$4 \times (0.8 \times 1.1$ m$^2)$
r_z	0.05 m	0.03 m
ρ	$\approx$1	$\approx$1
I_z	285 kg/m^2	70 kg/m^2
ω	15 rpm	10 rpm
$\xi_{\max}$	1.23 deg	1.60 deg

Although the torque model presented in the previous sections was established for a regular flat-surface element, it can readily be adapted to a cylindrical surface by considering N flat surfaces, each with a surface area of $hr_{\text{cyl}}\Delta\varphi$ with $\Delta\varphi = 2\pi/N$ (with N a large integer). When the cylinder has nearly homogeneous material properties, all of the N elements will have identical contributions to the resulting SRP torque. The total torque on the spacecraft is then found by summing the contributions of all N surface elements. Therefore, the total torque on a homogeneous cylindrical surface will be identical to that of a flat surface, with the same material properties and representative area $A = N(hr_{\text{cyl}}\Delta\varphi) = 2\pi hr_{\text{cyl}}$. After substituting the relevant input parameters into the torque expression of Eq. (46), we find the following useful result for the maximum attitude excursion from Eq. (52):

$$\xi_{\max} = 2Q/\omega_{\odot} \approx 8pAr_z/(3\pi I_z \omega\, \omega_{\odot}) \text{ [rad]} \tag{60}$$

The resulting maximum attitude-drift excursion for CONTOUR on the basis of the model of Eq. (60) and the inputs listed in Table 2 amounts to $\xi_{\max} = 1.23$ deg (see the last row of Table 2). This result indicates that the attitude drift induced by the solar radiation torque will stay well within acceptable limits throughout the hibernation periods.

An additional example is considered in the last column of Table 2: namely, a box-shaped minisatellite with relatively small dimensions. Most of the remaining inputs are taken identical to the conservative parameters adopted in the first example. The resulting maximum pointing excursion predicted by Eq. (60) is 1.60 deg. This indicates that the resulting attitude drift is not very sensitive to the specific satellite configuration parameters.

B. Long-Term Attitude Motion

Figure 5 shows the long-term evolution of the spacecraft spin axis over a full year, with the initial spin-axis orientation along the ecliptic north pole based on the CONTOUR inputs of Table 2. The analytical results are generated by MATLAB simulations using the ecliptic long-term model in Eq. (57). The results of the analytical model are virtually identical to those obtained from a numerical integration using MATLAB.

The figure shows the traces of the projected attitude vector in the plane normal to the ecliptic north pole. Two cases are shown, the first one starting at the vernal equinox and the second one starting at the summer solstice when the sun is 90 deg further ahead. The resulting spin-axis motion projected on the ecliptic plane is essentially circular with a period of 1 yr. The maximum spin-axis excursion (relative to the starting attitude) is about 1.23 deg and is reached after half a year. When considering different starting dates, the inertial direction of the spin-axis motion changes in accordance with the initial sun position within the ecliptic plane, but the maximum excursion is the same. The spin-axis motion starts out in an inertial direction that is 90 deg behind the initial sun position.

The case shown in Fig. 5 is unique because of the initial attitude pointing along the ecliptic north pole. This implies that the initial solar aspect angle $\gamma_0 = 90$ deg. In the absence of any attitude disturbance and control torques, the solar aspect angle would stay at 90 deg throughout the year [within the approximations of the adopted sun motion model of Eq. (2)]. Because the attitude variations induced by the SRP torques are relatively small, the average solar aspect angle γ_{ave} does not deviate far from 90 deg. In fact, the maximum change in

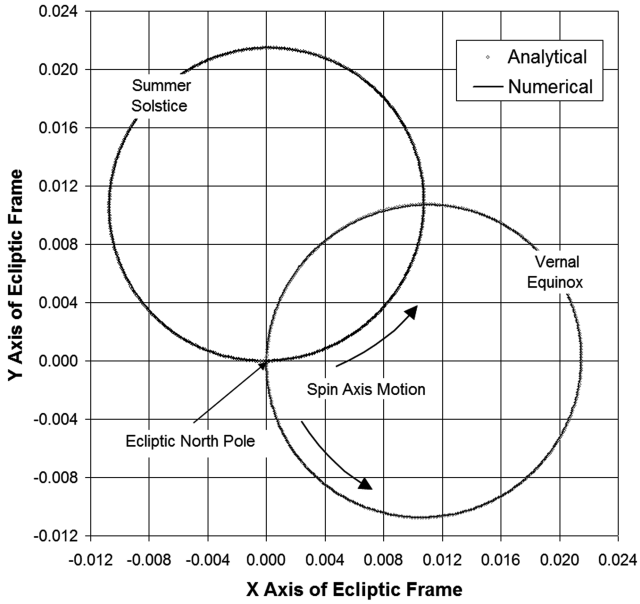

Fig. 5 Inertial motion of the spin axis with an initial attitude normal to the ecliptic.

solar aspect angle is equal to the maximum attitude excursion of 1.23 deg. Therefore, the approximate analytical results are extremely close (i.e., within 10^{-4} rad) to those of the exact numerical simulations over a period of about four years.

C. Spin Axis Normal to the Earth's Equator

We now consider the situation when the initial spin-axis orientation points along the Earth's equatorial north pole. Analytical results are generated by means of MATLAB simulations based on the general long-term model presented in Eq. (55). The accuracy of the analytical model is evaluated by means of a comparison with results from a numerical integration, as illustrated in Fig. 6.

Because of the effect of the ecliptic obliquity [Eqs. (2) and (3)], the initial solar aspect angle γ_0 now takes different values within the range of 66.56 to 113.44 deg, depending on the starting date. If the attitude were to stay fixed, the average solar aspect angle γ_{ave} over the year would still be 90 deg [within the approximations of the adopted

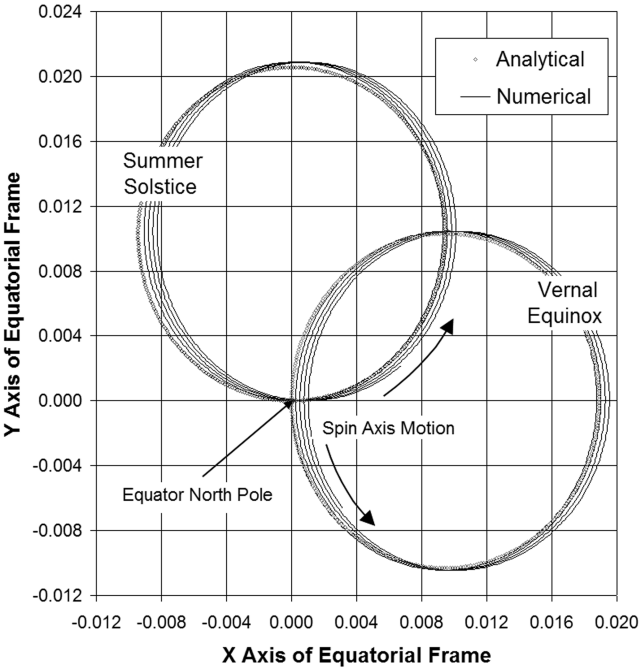

Fig. 6 Inertial motion of the spin axis with an initial attitude normal to the equator.

sun motion model of Eq. (2)]. This result is due to the fact that the average value of the dot product $\langle(\mathbf{z}\cdot\mathbf{s})\rangle$ vanishes over a year, as can be seen from Eqs. (2) and (3). It may be noted that the preceding statements are true for any fixed-attitude orientation. Because the attitude drift remains small, the average solar aspect angle will stay close to 90 deg, as in the previous case. On the other hand, however, the variations of the actual solar aspect angle about its average γ_{ave} value now have a relatively large amplitude of 23.44 deg and lead to the gradual divergence between the analytical and the numerical results over a time period of 1500 days, as illustrated in Fig. 6.

The maximum attitude excursion depends on the starting date (i.e., about 0.0189 rad or 1.08 deg for the vernal and autumnal equinoxes and 0.0206 rad or 1.18 deg for the two solstices). The difference is caused by the fact that the average SRP torque has a different magnitude over the first half-year interval for the two cases. The average solar aspect angle over the first half-year is 75.9 and 105.2 deg for the vernal and autumnal equinoxes and 90.6 and 90.5 deg for the summer and winter solstices, respectively. This fact also accounts for the elliptical shape of the resulting attitude motion, in contrast to the circular track in the previous case shown in Fig. 5.

Finally, it may be pointed out that for initial attitude orientations that are further away from the ecliptic pole than the equatorial case in Fig. 6, the variations in the solar aspect angle will be even larger and the long-term attitude tracks have a more elongated shape. In any case, the average sun angle will be 90 deg (for the sun motion model assumed here). The validity of the analytical model presented here will degrade during those periods when the deviation of the sun angle from its average value is relatively large.

VIII. Conclusions

A compact analytical model was established for predicting the long-term spin-axis attitude drift of a spin-stabilized spacecraft in the presence of solar radiation disturbance torques. A few illustrative practical examples with relevance to the attitude-pointing concept during hibernation periods were presented. The results demonstrate the periodic nature of the long-term spin-axis drift, which typically stays within acceptable excursion limits of 1 to 2 deg. The model can be used as a practical tool for better understanding of attitude motion and for designing attitude control concepts for future spacecraft and interplanetary probes. The results may also be useful for specific spacecraft design purposes (e.g., for predicting propellant needs for correction maneuvers based on specified spin-axis-pointing requirements).

References

[1] Sohn, R. L., "Attitude Stabilization by Means of Solar Radiation Pressure," *ARS Journal*, Vol. 29, No. 5, May 1959, pp. 371–373.

[2] Renner, U., "Attitude Control by Solar Sailing: A Promising Experiment with OTS-2," *ESA Journal*, Vol. 3, No. 1, 1979, pp. 35–40.

[3] Wie, B., "Dynamic Modeling and Attitude Control of Solar Sail Spacecraft, Part 1," *Journal of Guidance, Control, and Dynamics*, Vol. 27, No. 4, 2004, pp. 526–535.

[4] Wie, B., "Dynamic Modeling and Attitude Control of Solar Sail Spacecraft, Part 2," *Journal of Guidance, Control, and Dynamics*, Vol. 27, No. 4, 2004, pp. 536–544.

[5] Van der Ha, J. C., and Modi, V. J., "Analytical Evaluation of Solar Radiation Induced Orbital Perturbations of Space Structures," *The Journal of the Astronautical Sciences*, Vol. 25, No. 4, Oct.–Dec. 1977, pp. 283–306.

[6] Patterson, W., and Kissell, K., "Comparison of the Theoretical Solar Radiation Effects and the Observed Accelerations of the PAGEOS Satellite," *Journal of Spacecraft and Rockets*, Vol. 12, No. 9, 1975, pp. 539–543.

[7] Pande, K. C., "Attitude Control of Spinning Spacecraft by Radiation Pressure," *Journal of Spacecraft and Rockets*, Vol. 13, No. 12, 1976, pp. 765–768.

[8] Parvez, S. A., "Solar Pressure Disturbance on GSTAR and SPACENET Satellites," *Journal of Spacecraft and Rockets*, Vol. 31, No. 3, 1994, pp. 482–488.

[9] Ziebart, M., "Generalized Analytical Solar Radiation Modeling Algorithm for Spacecraft of Complex Shape," *Journal of Spacecraft and Rockets*, Vol. 41, No. 5, 2004, pp. 840–848.

[10] Rios-Reyes, L., and Scheeres, D. J., "Generalized Model for Solar Sails," *Journal of Spacecraft and Rockets*, Vol. 42, No. 1, 2005, pp. 182–185.

[11] Vallado, D. A., *Fundamentals of Astrodynamics and Applications*, 2nd ed., Kluwer Academic, Dordrecht, Holland, The Netherlands, 2001, pp. 265–269.

[12] Reynolds, E., Panneton, P., Reinhart, M., Mehoke, D., Dellinger, W., Williams, S., Perschy, J., Harvey, R., and Carr, P., "Use of Hibernation Modes for Deep Space Missions as a Method to Lower Operations Cost," 15th Small Satellite Conference, Logan, UT, Utah State Univ., Paper 01-8a-5, Aug. 2001.

[13] Wertz, J. R. (ed.), *Spacecraft Attitude Determination and Control*, Kluwer Academic, Dordrecht, Holland, The Netherlands, 1978, pp. 570–575.

[14] Van der Ha, J. C., "Models for Rhumb-Line Attitude Maneuvers and Error Propagation Effects," *Journal of Guidance, Control, and Dynamics*, Vol. 29, No. 6, Nov.–Dec. 2006, pp. 1384–1394.

[15] Wertz, J. R. (ed.), *Spacecraft Attitude Determination and Control*, Kluwer Academic, Dordrecht, Holland, The Netherlands, 1978, p. 652.